Dual-targeted Contrast Agent for US Assessment of Tumor Angiogenesis in Vivo[1]

Jürgen K. Willmann, MD
Amelie M. Lutz, MD
Ramasamy Paulmurugan, PhD
Manishkumar R. Patel, PhD
Pauline Chu, BA
Jarrett Rosenberg, PhD
Sanjiv S. Gambhir, MD, PhD

Purpose: To develop and validate a dual-targeted ultrasonographic (US) imaging agent with microbubbles (MBs) that attaches to both vascular endothelial growth factor (VEGF) receptor 2 (VEGFR2) and $\alpha_v\beta_3$ integrin and to compare the US imaging signal obtained from dual-targeted MBs (MB_D) with that from single-targeted MBs (MB_S) in a murine model of tumor angiogenesis.

Materials and Methods: Animal protocols were approved by the institutional Administrative Panel on Laboratory Animal Care. Single- and dual-targeted US imaging agents were prepared by attaching anti-VEGFR2, anti–$\alpha_v\beta_3$ integrin, or both antibodies to the shell of perfluorocarbon-filled MBs. Binding specificities of targeted MBs compared with isotype-matched immunoglobulin G–labeled control MBs (MB_C) and nontargeted nonlabeled MBs (MB_N) were tested with VEGFR2-positive and $\alpha_v\beta_3$ integrin–positive cells (mouse SVR cells) and control cells (mouse 4T1 cells). In vivo imaging signals of contrast material–enhanced US by using anti-VEGFR2–targeted MBs (MB_V), anti-$\alpha_v\beta_3$ integrin–targeted MBs (MB_I), MB_D, and MB_C were quantified in 49 mice bearing SK-OV-3 tumors (human ovarian cancer). Tumor tissue was stained for VEGFR2, $\alpha_v\beta_3$ integrin, and CD31.

Results: Attachment of MB_D to SVR cells (mean, 0.74 MBs per cell ± 0.05 [standard deviation]) was significantly higher than attachment to 4T1 cells (mean, 0.04 ± 0.03), and attachment to SVR cells was higher for MB_D than for MB_V (mean, 0.58 ± 0.09), MB_I (mean, 0.42 ± 0.21), MB_C (mean, 0.11 ± 0.13), and MB_N (mean, 0.01 ± 0.01) ($P < .05$). Imaging signal in the murine tumor angiogenesis model was significantly higher ($P < .001$) for MB_D (mean, 16.7 ± 7.2) than for MB_V (mean, 11.3 ± 5.7), MB_I (mean, 7.8 ± 5.3), MB_C (mean, 2.8 ± 0.9), and MB_N (mean, 1.1 ± 0.4). Immunofluorescence confirmed expression of VEGFR2 and $\alpha_v\beta_3$ integrin on tumor vasculature.

Conclusion: Dual-targeted contrast-enhanced US directed at both VEGFR2 and $\alpha_v\beta_3$ integrin improves in vivo visualization of tumor angiogenesis in a human ovarian cancer xenograft tumor model in mice.

Supplemental material: *http://radiology.rsnajnls.org/cgi/content/full/248/3/936/DC1*

[1] From the Molecular Imaging Program at Stanford, Department of Radiology and Bio-X Program (J.K.W., A.M.L., R.P., M.R.P., J.R., S.S.G.) and Department of Bioengineering (S.S.G.), Stanford University School of Medicine, the James H Clark Center, 318 Campus Dr, East Wing, 1st Floor, Stanford, CA 94305-5427; and Department of Comparative Medicine, Stanford University, Stanford, Calif (P.C.). Received December 31, 2007; revision requested February 15, 2008; revision received February 25; accepted March 6; final version accepted March 17. J.K.W. supported by the Swiss Foundation of Medical-Biological Grants, Novartis Research Foundation, and Swiss Society of Radiology. S.S.G. supported in part by National Cancer Institute Small Animal Imaging Resource Program; National Heart, Lung, and Blood Institute grant 1 R01 HL078632; National Cancer Institute In Vivo Cellular and Molecular Imaging Center grant CA114747 P50; and the Canary Foundation. **Address correspondence to** S.S.G. (e-mail: *sgambhir@stanford.edu*).

Angiogenesis, the formation and recruitment of new blood vessels from the host surrounding tissue, is an important process in early tumor progression (1). Most solid tumors require a switch to an angiogenic phenotype to provide sufficient oxygen, nutrients, and other growth factors to allow tumor growth beyond 1–2 mm (2–4). Several steps are involved in tumor angiogenesis, including proliferation, migration, and invasion of endothelial cells; formation of endothelial cells into tubular structures; maturation of blood vessels; and blood vessel degeneration (1). This complex process involves the coordination of several signal transduction pathways and is regulated by various proangiogenic and antiangiogenic molecules (5–7).

Vascular endothelial growth factor (VEGF) receptor 2 (VEGFR2) and $\alpha_v\beta_3$ integrin are two of the best-characterized molecular markers of tumor angiogenesis, and both are overexpressed on tumor endothelial cells during tumor angiogenesis. VEGFR2 is an endothelium-specific receptor tyrosine kinase, and activation of the VEGF/VEGFR2 axis triggers multiple signaling networks that result in endothelial cell survival, mitogenesis, migration, and differentiation, as well as altered vascular permeability (1). The $\alpha_v\beta_3$ integrin is a heterodimeric transmembrane receptor for extracellular matrix molecules, including fibronectin, fibrinogen, von Willebrand factor, vitronectin, and proteolysed forms of collagen and laminin (8,9). These extracellular matrix molecules activate signaling cascades that regulate gene expression, cytoskeletal organization, cell adhesion, and cell survival, with the result of making cancer cells more invasive, more migratory, and better able to survive in different microenvironments (8).

Because of their pivotal role in tumor growth and migration, both VEGFR2 and $\alpha_v\beta_3$ integrin have been selected as targets for therapeutic strategies that are now being successfully introduced clinically in cancer patients. Inhibition of the VEGF/VEGFR2 pathway with the humanized antibody bevacizumab, in combination with chemotherapy, results in a survival advantage in patients with previously untreated metastatic colorectal cancer and nonsquamous non–small cell lung carcinoma relative to chemotherapy alone (10,11). The small-molecule VEGFR tyrosine kinase inhibitors sunitinib and sorafenib have shown effectiveness in the treatment of metastatic renal cell cancer patients and were recently approved by the Food and Drug Administration (12, 13). In addition, the humanized anti–$\alpha_v\beta_3$ integrin antibody etaracizumab has demonstrated prolongation of stable disease in patients with renal cell carcinoma in a phase I clinical study (14).

Noninvasive imaging strategies for the detection and quantification of molecular markers of tumor angiogenesis may be particularly helpful for the tracking of antiangiogenic and tumoricidal treatments in cancer patients, for the diagnosis of cancer at early stages, and in the de novo development of cancer therapeutics in preclinical animal studies. Targeted contrast agents have been introduced for ultrasonography (US) that allow accurate visualization and quantification of molecular markers of tumor angiogenesis (15–17). These US contrast agents are gas-filled, echogenic microspheres (microbubbles [MBs]) that can be directed to vascular molecular targets by the attachment of target-specific ligands to the shell of the MBs. After systemic administration, these functionalized MBs attach at vascular sites, overexpressing the molecular markers for which the attached ligands are specific, and produce an increase in the US imaging signal.

In the current study, we hypothesized that contrast material–enhanced US by using a newer imaging agent, dual-targeted MBs (MB_D) directed at both VEGFR2 and $\alpha_v\beta_3$ integrin in tumor angiogenesis, would result in more enhanced US imaging signal than that with traditional single-targeted contrast agents. Thus, the purpose of our study was to develop and validate a dual-targeted US imaging agent, MB_D, that attaches to both VEGFR2 and $\alpha_v\beta_3$ integrin and to compare the US imaging signal obtained from this MB_D with that obtained from single-targeted MBs (MB_S) in a murine model of tumor angiogenesis.

Advances in Knowledge

- Contrast agent microbubbles (MBs) can be modified to attach to both vascular endothelial growth factor (VEGF) receptor 2 (VEGFR2) and $\alpha_v\beta_3$ integrin.
- Dual-targeted MBs (MB_D), targeting both VEGFR2 and $\alpha_v\beta_3$ integrin, increase the imaging signal of targeted contrast-enhanced US compared with single-targeted MBs in a murine model of tumor angiogenesis.

Implication for Patient Care

- The increased imaging signal of contrast-enhanced US by using MB_D may facilitate its future application for cancer diagnosis and monitoring of cancer treatment in patients.

Published online
10.1148/radiol.2483072231

Radiology 2008; 248:936–944

Abbreviations:
ICAM-1 = intercellular adhesion molecule 1
MB = microbubble
MB_C = control MBs
MB_D = dual-targeted MBs
MB_I = anti-$\alpha_v\beta_3$ integrin–targeted MBs
MB_N = nontargeted nonlabeled MBs
MB_S = single-targeted MBs
MB_V = anti-VEGFR2–targeted MBs
VEGF = vascular endothelial growth factor
VEGFR2 = VEGF receptor 2

Author contributions:
Guarantors of integrity of entire study, J.K.W., A.M.L., S.S.G.; study concepts/study design or data acquisition or data analysis/interpretation, all authors; manuscript drafting or manuscript revision for important intellectual content, all authors; manuscript final version approval, all authors; literature research, J.K.W.; experimental studies, J.K.W., A.M.L., R.P., M.R.P., P.C.; statistical analysis, J.K.W., J.R., S.S.G.; and manuscript editing, J.K.W., A.M.L., R.P., S.S.G.

See Materials and Methods for pertinent disclosures.

Materials and Methods

VisualSonics (Toronto, Ontario, Canada) provided the MBs used in this study. All authors who are not consultants for VisualSonics had control of inclusion of any data and information that might present a conflict of interest for the author (S.S.G.) who is a consultant for VisualSonics.

The description of the preparation of functionalized MBs, as well as of cell culture experiments for testing binding specificity of MB_S and MB_D to both VEGFR2 and $\alpha_v\beta_3$ integrin is detailed in Appendix E1 (*http://radiology.rsnajnls.org/cgi/content/full/248/3/936/DC1*).

In Vivo Small-Animal Imaging Experiments

Mouse tumor models.—Animal protocols were approved by the institutional Administrative Panel on Laboratory Animal Care. Subcutaneous human ovarian adenocarcinoma xenograft tumors were established in 49 female 6–8-week-old nude mice (Charles River Laboratories, Wilmington, Mass) by means of subcutaneous injection of 3×10^6 SK-OV-3 cells in 50 μL of phosphate-buffered saline into the right flank region. During the injections, the mice were anesthetized with 2% isoflurane (Aerrane; Baxter, Deerfield, Ill) in oxygen administered at a rate of 2 L/min. Tumors were allowed to grow to a mean maximum diameter of 3.0 mm (range, 2.2–3.4 mm).

Targeted contrast-enhanced US.—One radiologist (J.K.W., with 8 years of experience in performing US) performed real-time (20-Hz), two-dimensional fundamental brightness–mode (B-mode) targeted contrast-enhanced US by using a dedicated small-animal high-resolution imaging system (Vevo 770; VisualSonics) and a 40-MHz high-frequency linear transducer (RMV-704; VisualSonics). Lateral and axial resolution were 100 and 40 μm, respectively; focal length was 6 mm; transmit power was 50%; mechanical index was 0.14; and dynamic range was 52 dB. The transducer was fixed on a railing system to maintain the acoustic focus centered at the level of the largest transverse cross section of the subcutaneous tumors. In the animals, anesthesia was maintained during imaging with 2% isoflurane in oxygen administered at a rate of 2 L/min, and the body temperature was kept constant at 37°C by using a heating pad and a warming lamp. B-mode settings (gain, time gain compensation) were kept constant throughout each imaging session. In the first subgroup of 18 tumor-bearing mice, 5×10^7 MB_D, 5×10^7 anti-VEGFR2–targeted MBs (MB_V), and 5×10^7 anti-$\alpha_v\beta_3$ integrin–targeted MBs (MB_I) were injected manually through the tail vein in random order (MB volume, 60 μL per injection; injection time, 3 seconds) during the same imaging session. A pause of 30 minutes was chosen between each injection to allow clearance of MBs from the vasculature (18).

By using the following destruction-replenishment imaging sequence (17), targeted contrast-enhanced US was then performed: Two hundred forty seconds after each MB injection (to allow targeted MBs to attach to endothelial molecular markers), 120 imaging frames were acquired during 6 seconds with the imaging parameters described previously. A continuous (10-MHz) high-power destructive pulse (mechanical index, approximately 0.235; average power, approximately 0.0676 W/cm^2) was then applied for 3 seconds to destroy all MBs within the beam elevation. Following destruction (9 seconds were given to allow freely circulating MBs to refill into tumor vessels), another 120 imaging frames were acquired. The imaging signals (video intensity) from these 120 imaging frames were averaged to compensate for slight breathing motion artifacts and were digitally subtracted from the initial 120 predestruction frames. The resulting difference in video intensity corresponds to the imaging signal attributable to MBs adherent to molecular endothelial markers (17–19). In the same 18 tumor-bearing mice, targeted US of normal skeletal muscle (hind limb adductor muscles as a quasi tumor angiogenesis–negative model) was performed as described previously for tumor imaging to assess contrast enhancement of nonneoplastic and nonangiogenic microvasculature after injection of MB_D, MB_V, and MB_I. To test the specificity of signal coming from MBs attached to VEGFR2 and $\alpha_v\beta_3$ integrin, respectively, 5×10^7 isotype-matched immunoglobulin G–labeled control MBs (MB_C) and 5×10^7 nontargeted nonlabeled MBs (MB_N) were also injected in random order in the same 18 tumor-bearing mice during the same imaging sessions.

To test whether there was a difference in video intensity when scanning with MB_D as opposed to scanning with a mixture of both MB_V and MB_I (with theoretically the same absolute number of binding ligands as the MB_D), we scanned an additional subgroup of 11 tumor-bearing mice after the administration in random order of 5×10^7 MB_D and a mixture of 2.5×10^7 MB_V and 2.5×10^7 MB_I.

To further test the specificity of the signal coming from MBs attached to endothelial VEGFR2 and $\alpha_v\beta_3$ integrin, in vivo dual-blocking studies were performed in another subgroup of 10 tumor-bearing mice. First, mice were injected with 5×10^7 MB_D and were imaged by using the previously described imaging sequence. After 30 minutes to allow clearance of MBs from the blood circulation, a mixture of 125 μg of rat antimouse VEGFR2 and 125 μg of rat antimouse α_v monoclonal antibodies (eBioscience, San Diego, Calif), for a total of 500 μL, was injected manually through the tail vein within 1 minute. After 30 minutes to allow distribution of the two types of antibodies in the tissue, targeted US by using 5×10^7 MB_D was repeated. In another subset of 10 tumor-bearing mice, sequential in vivo single-blocking experiments were performed. For this purpose, the blocking monoclonal antimouse VEGFR2 antibody (eBioscience), for a total of 125 μg, was injected first, and then imaging with MB_D was performed after 30 minutes. Thereafter, antimouse α_v antibody (eBioscience), for a total of 250 μL, was injected intravenously, and imaging with MB_D was repeated after 30 minutes.

Image Analysis

After imaging, frames were recorded digitally and analyzed off-line by using commercially available high-resolution

micro-US software (Vevo 770; VisualSonics). One radiologist performed image analysis in random order and was blinded to the types of administered MBs. In regions of interest drawn over the whole tumor in the two-dimensional imaging planes, average image brightness (video intensity, which corresponds to the 8-bit log-compressed gray scale) was measured, and the difference in video intensity from subtraction of the pre- and postdestruction image frames (described previously) was automatically displayed by the software as a color (green) overlay on the B-mode anatomic images. In hind limb muscles, regions of interest were set to encompass the adductor muscle.

Ex Vivo Immunofluorescence Staining of Tumors

Animals were euthanized after US, and the subcutaneous tumors were excised, embedded in optimal cutting temperature compound (Sakura Finetek, Torrance, Calif), and frozen on dry ice. Frozen blocks were sectioned at 10 μm and mounted on glass slides for immunofluorescence staining. A double-staining procedure was employed to visualize VEGFR2 and $\alpha_v\beta_3$ integrin expression on tumor endothelial cells. The following were used for mouse VEGFR2 staining: a rabbit antimouse VEGFR2 primary antibody, with dilution of 1:500 (Thermo Fisher Scientific, Waltham, Mass); a biotinylated goat antirabbit secondary antibody, with dilution of 1:500 (Jackson ImmunoResearch Laboratories, West Grove, Pa); and streptavidin labeled with a dye (AlexaFluor 594; Invitrogen, Carlsbad, Calif), with dilution of 1:200. The following were used for staining of mouse $\alpha_v\beta_3$ integrin: a hamster antimouse β_3 primary antibody (BD Bioscience, San Jose, Calif), with dilution of 1:100; a biotinylated mouse antihamster secondary antibody, with dilution of 1:300 (BD Bioscience); and streptavidin labeled with the same dye as was used for mouse VEGFR2 staining, with dilution of 1:200. Slices were double stained for mouse CD31 by using a rat antimouse CD31 primary antibody (BD Bioscience), with dilution of 1:100; a biotinylated goat antirat secondary antibody (Jackson ImmunoResearch Laboratories), with dilution of 1:500; and streptavidin labeled with the same dye as was used for mouse VEGFR2 staining, with dilution of 1:200. Fluorescent images were acquired with microscopy (Axiophot; Carl Zeiss, Thornwood, NY) and were documented with a digital camera (AxioCam MRc; Carl Zeiss, Bernried, Germany).

Statistical Analysis

Data are reported as the mean ± standard deviation. For cell culture experiments, a 2 × 2 × 2 between-groups analysis of variance was performed on cell attachment rates of MBs with factors of the type of cell line (SVR or 4T1) and VEGFR2 and $\alpha_v\beta_3$ integrin targeting of MBs. Differences in cell attachments of MB_D with and without addition of blocking antibodies were assessed by

Figure 1

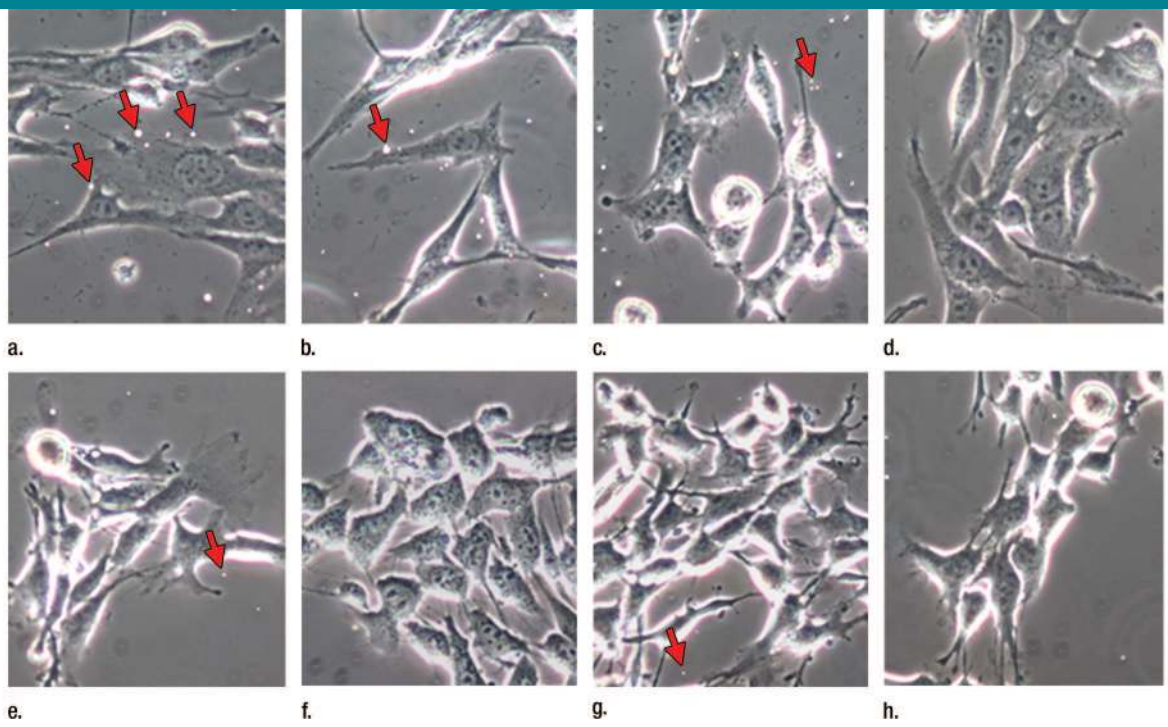

Figure 1: Light microscopic images of **(a–d)** SVR cells and **(e–h)** control 4T1 cells after static incubation with MB_D on **a** and **e**, MB_V on **b** and **f**, MB_I on **c** and **g**, and MB_C on **d** and **h**. MB_D, MB_V, and MB_I attached to SVR cells but rarely to 4T1 cells. MB_C rarely attached to either type of cells. Small rounded structures are MBs (arrows), which can be counted to obtain the number of attached MBs per cell. Quantitation is given in the Table. (Original magnification, ×400.)

using the Mann-Whitney test. To assess the effect of MB type on video intensity in in vivo experiments, a 2 × 2 × 2 repeated-measures analysis of variance was performed with within-subject factors of VEGFR2 targeting, $\alpha_v\beta_3$ integrin targeting, and tissue type (SK-OV-3 tumor vs nonneoplastic and nonangiogenic microvasculature in normal skeletal muscle tissue). In addition, paired Wilcoxon signed rank tests were used to test differences in video intensity for all in vivo imaging studies in the same animals. All statistical analyses were performed with software (Stata 9.2; Stata, College Station, Tex). A difference with a *P* value of less than .05 was considered significant.

Results

Cell Attachment Studies

At flow cytometry, expression of both mouse VEGFR2 and $\alpha_v\beta_3$ integrin on SVR cells was observed, whereas 4T1 cells were negative for mouse VEGFR2 and only slightly positive for mouse $\alpha_v\beta_3$ integrin. Attachment of MB_S and MB_D to SVR cells was significantly higher ($P < .01$) than attachment to negative control 4T1 cells (Fig 1, Table). Both MB_C and MB_N adhered only minimally to SVR cells. After preincubation of SVR cells with antimouse VEGFR2 and antimouse α_v antibodies, attachment of MB_D to SVR cells was significantly ($P < .05$) reduced (Table).

In Vivo Small-Animal Imaging Experiments

In all animals, there were no signs of any acute toxic reactions after MB administration, and all animals fully recovered after the US imaging sessions.

A VEGFR2-specific or $\alpha_v\beta_3$-integrin–specific imaging signal was measured in all tumors by using contrast-enhanced US after administration of MB_S. On average, the mean difference in video intensity was 11.3 ± 5.7 after administration of MB_V and 7.8 ± 5.3 after administration of MB_I in the first group of 18 tumor-bearing mice. In the same imaging session and in the tumors of the same animals, the difference in video intensity significantly increased ($P < .001$) after administration of MB_D, with a mean difference in video intensity of 16.7 ± 7.2 (Fig 2). To confirm binding specificity of MB_V and MB_I, MB_C were administered in the same an-

Attachment of Different Types of MBs to Mouse Angiosarcoma (SVR) Cells and Mouse Breast Cancer (4T1) Cells in Cell Culture Experiments

Cell Line and Type of MBs	Adherent MBs per Cell	
	Mean	Standard Deviation
SVR		
MB_D	0.74	0.05
MB_D and blocking	0.09	0.09
MB_V	0.58	0.09
MB_I	0.42	0.21
MB_C	0.11	0.13
MB_N	0.01	0.01
4T1		
MB_D	0.04	0.03
MB_D and blocking	0.02	0.0003
MB_V	0.01	0.001
MB_I	0.04	0.01
MB_C	0.03	0.02
MB_N	0.01	0.02

Note.—Blocking was performed with preincubation with anti-VEGFR2 and anti-α_v integrin antibodies. MB_D consists of VEGFR2-targeted and $\alpha_v\beta_3$ integrin–targeted MBs; MB_N consists of nonlabeled control MBs.

Figure 2

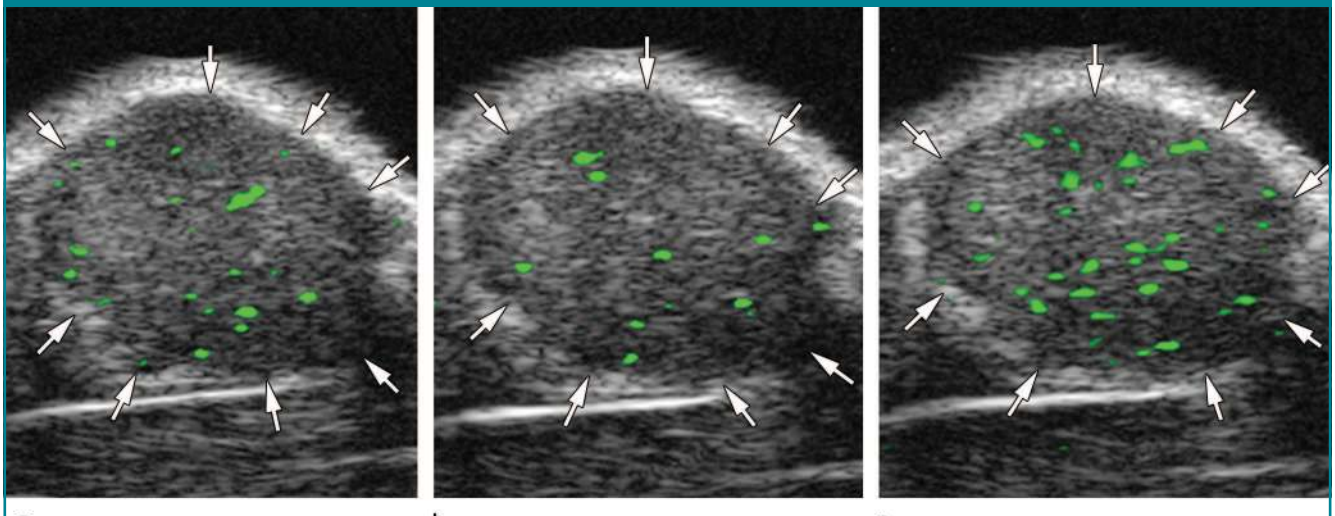

Figure 2: Transverse color-coded US images in subcutaneous human ovarian adenocarcinoma (SK-OV-3) xenograft tumor (arrows) from nude mouse. Imaging was performed in same imaging session 4 minutes after intravenous injection of **(a)** MB_V, **(b)** MB_I, or **(c)** MB_D, with 30 minutes between injections to allow clearance of previously injected MBs. Difference in video intensity (color-coded as green signal from adherent MBs on gray-scale US images) was highest after administration of MB_D in this tumor.

imals in the same imaging session, and contrast-enhanced US of the same tumors was again performed. Differences in video intensity were significantly decreased ($P < .001$) after administration of both MB_C (mean, 2.8 ± 0.9) and MB_N (mean, 1.1 ± 0.4). In another experiment with a second group of 11 tumor-bearing mice, the mean difference in video intensity after administration of MB_D was 15.9 ± 7.8, which was significantly higher ($P < .05$) compared with the mean difference in video intensity after administration of the mixture of both MB_V and MB_I (10.2 ± 4.7).

To further confirm binding specificity of MB_D to both VEGFR2 and $\alpha_v\beta_3$ integrin, in vivo–blocking experiments were performed in another group of 10 tumor-bearing mice. After simultaneous administration of both antimouse VEGFR2 and antimouse α_v antibodies, the mean difference in video intensity after administration of MB_D significantly decreased ($P < .005$) from 15.6 ± 8.3 before blocking to 8.5 ± 7.8 after blocking (Fig 3). In another subset of 10 tumor-bearing animals, sequential in vivo blocking of both VEGFR2 and α_v was performed. The mean difference in video intensity after administration of MB_D significantly decreased ($P < .018$) from 17.6 ± 7.7 to 8.9 ± 4.4 after VEGFR2 blocking and significantly decreased further ($P < .018$) to 4.1 ± 2.6 after additional α_v blocking and additional imaging with MB_D in the same imaging session (Fig 4).

Finally, as a quasi tumor angiogenesis–negative model, nonneoplastic and nonangiogenic vasculature in normal skeletal muscle tissue was imaged after administration of MB_D, MB_V, and MB_I. For all three types of targeted MBs, mean differences in video intensity measured over skeletal muscle tissue (MB_D, 1.05 ± 0.48; MB_V, 1.1 ± 0.51; MB_I, 1.14 ± 0.48) were significantly smaller ($P < .001$) compared with those measured over tumor tissue.

Figure 3

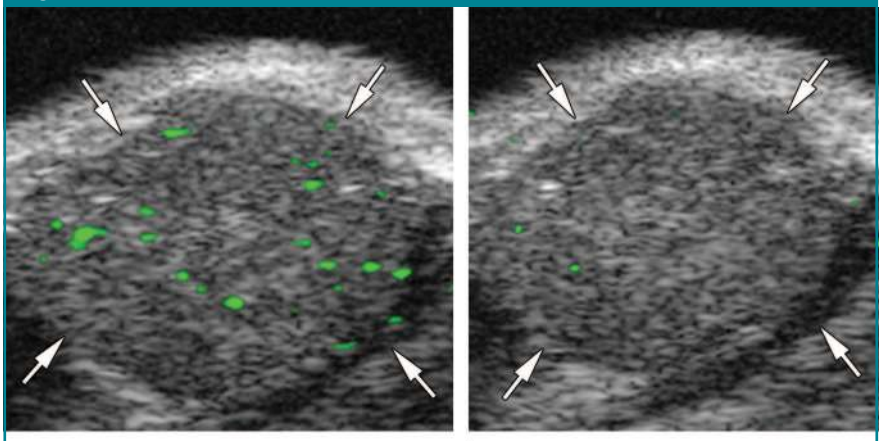

a. b.

Figure 3: Transverse color-coded US images of subcutaneous human ovarian adenocarcinoma (SK-OV-3) xenograft tumor (arrows) in nude mouse after intravenous injection of MB_D either **(a)** without or **(b)** with administration of mixture of anti-VEGFR2 and anti-α_v antibodies 30 minutes before MB injection. Difference in video intensity, shown as green areas overlaid on gray-scale images, was substantially reduced with administration of blocking antibodies.

Ex Vivo Immunofluorescence Staining of Tumors

After US, tumors were excised and tumor slices were double stained for mouse VEGFR2 and CD31, as well as for mouse $\alpha_v\beta_3$ integrin and CD31. CD31 was used as a marker of vascular endothelium. Immunofluorescence showed colocalization of both VEGFR2 and β_3 with CD31, confirming presence of both mouse VEGFR2 and $\alpha_v\beta_3$ integrin on endothelial cells within the SK-OV-3 tumors in our study (Fig 5).

Discussion

In this study, we demonstrated that MBs that were dually targeted to both mouse VEGFR2 and mouse $\alpha_v\beta_3$ inte-

Figure 4

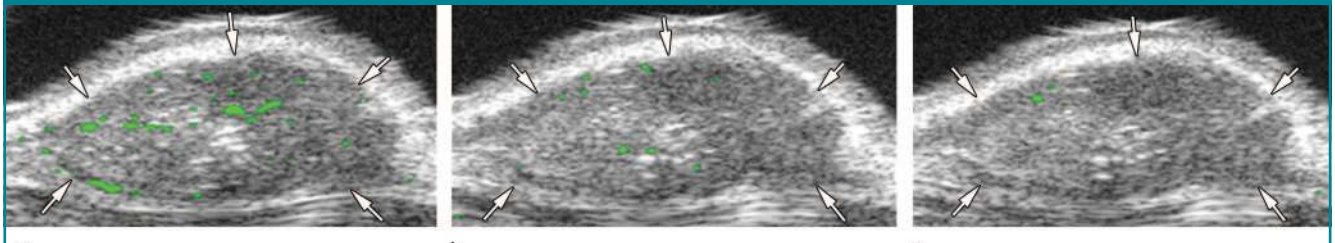

a. b. c.

Figure 4: Transverse color-coded US images of subcutaneous human ovarian adenocarcinoma (SK-OV-3) xenograft tumor (arrows) obtained with MB_D **(a)** before, **(b)** 30 minutes after blocking with anti-VEGFR2 antibodies, and **(c)** 30 minutes after blocking with additional anti-α_v antibodies. Signal from adherent MB_D, visualized as green areas overlaid on gray-scale images, was substantially reduced after administration of anti-VEGFR2 and was further decreased after injection of anti-α_v antibodies. MB_D were administered in all three experiments; imaging was performed after 4-minute delay.

grin led to higher levels of attachment and resultant US imaging signal than either of the single-targeted MBs at sites of tumor angiogenesis in tumor-bearing mice.

Few studies have addressed the assessment of tumor angiogenesis with targeted contrast-enhanced US. By using echistatin as the binding ligand on the MB shell, an α_v-specific signal in an orthotopic malignant glioblastoma tumor model in rats has been demonstrated by using targeted contrast-enhanced US (15). By coupling monoclonal antibodies against endoglin, VEGFR2, or VEGF-activated blood vessels on the MB surface, tumor angiogenesis during treatment of subcutaneous and orthotopic pancreatic tumors has been monitored by using targeted contrast-enhanced US (16). Recently, tumor angiogenesis has been visualized by using targeted contrast-enhanced US in rat glioblastoma and mouse angiosarcoma tumor models by using MBs coupled to monoclonal antibodies targeted to VEGFR2 (17). In all three studies, the imaging signal measured was from MBs attached to a single marker of tumor angiogenesis. However, contrast agents binding to more than one molecular marker may be advantageous over single-targeted contrast agents by increasing the number of MBs attached at sites of tumor angiogenesis. This may enhance the specific US signal from tumor angiogenesis and, hence, may facilitate cancer detection and cancer treatment monitoring in vivo. We hypothesized that targeting two major markers of tumor angiogenesis, VEGFR2 and $\alpha_v\beta_3$ integrin, could lead to an increase in MB attachment to tumor vessels and, thus, could improve US depiction and quantification of tumor angiogenesis.

In the current study, we first addressed binding specificity of MB_D to both VEGFR2 and $\alpha_v\beta_3$ integrin in cell culture experiments. MB_D adhered more to VEGFR2-positive and $\alpha_v\beta_3$ integrin–positive cells than did MB_S, MB_V, and MB_I. We then tested the different types of MBs in vivo by using human ovarian cancer (SK-OV-3) xenograft tumors in mice and showed higher imaging signal when we used MB_D compared with MB_S. To ensure a direct intraindividual comparison between video intensities derived from the contrast agents in our study, the MBs were injected consecutively in the same animals during the same imaging sessions, and US of the almost identical two-dimensional imaging plane was performed with all imaging settings kept constant. To further obviate any bias from the order of MB injections and to minimize interactions between the MB types, the different MBs were administered in random order, and a delay of 30 minutes between the MB injections was used. We chose this delay between MB injections on the basis of our experience (20), as well as that of others (18), that most of the MBs are cleared from the mouse vasculature within 30 minutes after intravenous injection.

The concept of MB_D has been evaluated in cell culture experiments with the use of MBs targeted at two inflammation markers, intercellular adhesion molecule 1 (ICAM-1) and selectin (21). Inflammation of human coronary artery endothelial cells was induced by activation with interleukin 1β, and the cells were then incubated with MBs labeled with antihuman ICAM-1 antibody, natural selectin ligand sialyl Lewis^X, or with a combination of the two (21). By using a radial flow chamber to quantify the adhesion strength of the types of MBs, it has been demonstrated that the mean

Figure 5

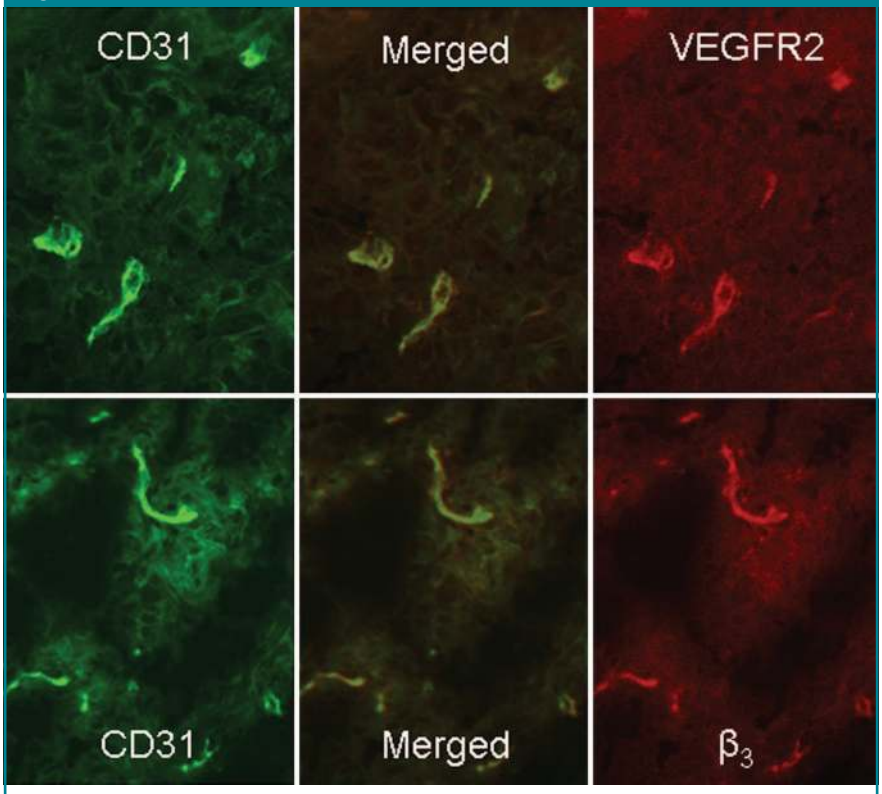

Figure 5: Immunofluorescence staining of human ovarian adenocarcinoma (SK-OV-3) tumor slices for VEGFR2, β_3 integrin subunit, and CD31. CD31 is expressed on vascular endothelium. Immunofluorescence images of mouse CD31 (green), mouse VEGFR2 (red), and merged VEGFR2- and CD31-stained image (yellow) demonstrate expression of VEGFR2 on endothelial cells in SK-OV-3 tumors (top). Mouse β_3 is also colocalized on endothelial cells of tumor blood vessels in SK-OV-3 tumors as evidenced by immunofluorescence staining of another tumor slice (bottom) for CD31 and β_3, and on merged β_3- and CD31-stained image (yellow on merged image confirms colocalization). CD31 was visualized with dye (AlexaFluor 488; Invitrogen) (green); VEGFR2 and β_3 were visualized with dye (AlexaFluor 594; Invitrogen) (red). (Original magnification, ×400).

critical shear rate of MB_D (440/sec ± 90) was significantly greater than that of both ICAM-1–targeted (340/sec ± 70) and selectin-targeted (370/sec ± 70) MBs (21).

In our study, we add to these experiments (21) by introducing for the first time, to our knowledge, a US contrast agent that is based on MB_D targeted to tumor angiogenesis. These MBs were directed at two major regulators of angiogenesis, VEGFR2 and $\alpha_v\beta_3$ integrin. Our study is clinically important in that we tested for the first time, to our knowledge, MB_D in living animals. In our study, there was a substantial increase in video intensity after administration of MB_D compared with MB_S. There may be several explanations for this increase of signal in vivo. First, it might be intuitively expected that two ligands directed to two different markers on the endothelial cells may increase the likelihood of MB attachment because each MB can bind to an increased number of targets. The extent of signal enhancement, thereby, depends on the number of targets in the tumor vessels, the numeric distribution of the markers on the endothelial cells, as well as on the absolute and relative number of the two binding ligands on the MB shell. Because various tumor types may express different levels of both VEGFR2 and $\alpha_v\beta_3$ integrin on tumor vasculature, and these levels also may change during tumor progression, the absolute values of increased video intensity in our human ovarian cancer tumor model may, therefore, not be directly generalizable to other tumor types or other tumor stages.

Another explanation for a signal increase after administration of MB_D may be a synergistic interaction between the two binding ligands in our study. For example, it might be possible that binding of one of the ligands, even if only temporarily, could first capture the MB to the target surface or slow down the moving MB, allowing the second binding ligand to also attach to the endothelium, thereby increasing the bonding interactions and the probability of the MB to actually adhere to the tumor endothelial cells.

This mechanism of synergistic interactions has been found to be likely between two binding ligands with different attachment strengths and has been modeled for leukocytes binding on inflammatory endothelial cells through the two molecular markers ICAM-1 (mediating strong attachment) and selectin (mediating weak attachment) (22). In a recent in vitro study, polystyrene microspheres were functionalized with the two binding ligands P-selectin and ICAM-1, and a synergistic interaction between the two binding ligands with an increased attachment of the microspheres to a P-selectin and ICAM-1 surface was found (23). Future studies with the use of optical systems, such as intravital microscopy, may allow direct in vivo visualization of fluorescent-labeled MBs passing through tumor vessels. This factor may help to define different binding patterns of functionalized MBs on tumor endothelial cells and may be instrumental in the prediction of signal enhancement by using US contrast agents such as MB_D or multitargeted MBs.

An increase in sensitivity by using MB_D may be particularly helpful for future molecular US imaging in cancer types with low VEGFR2 or $\alpha_v\beta_3$ integrin expression levels, such as early-stage cancer containing only a small number of tumor vessels. In particular, for future cancer screening approaches, the use of MB_D with increased imaging signal may be advantageous when US, in combination with a panel of different screening serum biomarkers, is performed as a second step for detection and further characterization of a suspicious lesion in certain organs such as the ovaries. Further studies are warranted to address the specificity of targeted contrast-enhanced US in imaging tumor angiogenesis in this clinical scenario. A direct comparison between imaging techniques by using low-frequency US (as used in clinical applications) versus high-frequency US (as used for small-animal imaging) is also needed to address differences in imaging signal related to technical approaches of targeted contrast-enhanced US.

The following limitations of the study need to be addressed. The imaging approach described in our study allowed visualization of tumor angiogenesis only within the small width of the transducer beam. Therefore, in inhomogeneous tumor tissues, the imaging signal derived by using targeted contrast-enhanced US depends on the positioning of the transducer on the tumor, which limits the repeatability of studies even in the same animal. Further developments in three-dimensional imaging techniques that allow quantification of expression levels of molecular markers within the entire tumor volume are needed. In addition, although we administered the different types of MBs in random order, we cannot exclude some confounding interactions from repetitive contrast agent administration within the same animal, which may have influenced the absolute values of video intensities obtained in our study. Additional studies in which the influence of MB doses on imaging signal is addressed and in which the sensitivity of dual-targeted US is compared with that of other quantitative molecular imaging modalities are warranted and will further help define the role of targeted contrast-enhanced US in oncologic imaging.

In conclusion, the results of our study suggest that dual-targeted contrast-enhanced US targeting both VEGFR2 and $\alpha_v\beta_3$ integrin improves in vivo visualization of tumor angiogenesis in a human ovarian cancer xenograft tumor model in mice.

Because of its wide clinical availability, noninvasiveness, real-time high-spatial-resolution imaging capabilities, and lack of ionizing radiation, targeted contrast-enhanced US is an attractive approach for high-throughput molecular imaging. These features may also simplify the translation of this imaging approach from preclinical animal models to clinical applications in patients in the near future. The enhanced imaging signal at sites of tumor angiogenesis produced by using MB_D may be useful in cases such as the early detection of cancer when tumors are too small to cause detectable morphologic changes but

large enough to induce tumor angiogenesis. Sensitive quantification of tumor angiogenesis with US by using MB_D also may be a valuable tool for future monitoring of antiangiogenic strategies when whole-body imaging is not needed.

References

1. Hicklin DJ, Ellis LM. Role of the vascular endothelial growth factor pathway in tumor growth and angiogenesis. J Clin Oncol 2005; 23:1011–1027.
2. Folkman J. Tumor angiogenesis: therapeutic implications. N Engl J Med 1971;285:1182–1186.
3. Naumov GN, Akslen LA, Folkman J. Role of angiogenesis in human tumor dormancy: animal models of the angiogenic switch. Cell Cycle 2006;5:1779–1787.
4. Fidler IJ, Ellis LM. The implications of angiogenesis for the biology and therapy of cancer metastasis. Cell 1994;79:185–188.
5. Bergers G, Benjamin LE. Tumorigenesis and the angiogenic switch. Nat Rev Cancer 2003; 3:401–410.
6. Hanahan D, Weinberg RA. The hallmarks of cancer. Cell 2000;100:57–70.
7. Nyberg P, Xie L, Kalluri R. Endogenous inhibitors of angiogenesis. Cancer Res 2005; 65:3967–3979.
8. Hood JD, Cheresh DA. Role of integrins in cell invasion and migration. Nat Rev Cancer 2002;2:91–100.
9. van der Flier A, Sonnenberg A. Function and interactions of integrins. Cell Tissue Res 2001;305:285–298.
10. Hurwitz H, Fehrenbacher L, Novotny W, et al. Bevacizumab plus irinotecan, fluorouracil, and leucovorin for metastatic colorectal cancer. N Engl J Med 2004;350:2335–2342.
11. Sandler A, Gray R, Perry MC, et al. Paclitaxel-carboplatin alone or with bevacizumab for non-small-cell lung cancer. N Engl J Med 2006;355:2542–2550.
12. Escudier B, Eisen T, Stadler WM, et al. Sorafenib in advanced clear-cell renal-cell carcinoma. N Engl J Med 2007;356:125–134.
13. Motzer RJ, Hutson TE, Tomczak P, et al. Sunitinib versus interferon alfa in metastatic renal-cell carcinoma. N Engl J Med 2007; 356:115–124.
14. McNeel DG, Eickhoff J, Lee FT, et al. Phase I trial of a monoclonal antibody specific for alphavbeta3 integrin (MEDI-522) in patients with advanced malignancies, including an assessment of effect on tumor perfusion. Clin Cancer Res 2005;11:7851–7860.
15. Ellegala DB, Leong-Poi H, Carpenter JE, et al. Imaging tumor angiogenesis with contrast ultrasound and microbubbles targeted to alpha(v)beta3. Circulation 2003;108:336–341.
16. Korpanty G, Carbon JG, Grayburn PA, Fleming JB, Brekken RA. Monitoring response to anticancer therapy by targeting microbubbles to tumor vasculature. Clin Cancer Res 2007;13:323–330.
17. Willmann JK, Paulmurugan R, Chen K, et al. US imaging of tumor angiogenesis with microbubbles targeted to vascular endothelial growth factor receptor type 2 in mice. Radiology 2008;246:508–518.
18. Weller GE, Wong MK, Modzelewski RA, et al. Ultrasonic imaging of tumor angiogenesis using contrast microbubbles targeted via the tumor-binding peptide arginine-arginine-leucine. Cancer Res 2005;65:533–539.
19. Lindner JR, Song J, Xu F, et al. Noninvasive ultrasound imaging of inflammation using microbubbles targeted to activated leukocytes. Circulation 2000;102:2745–2750.
20. Willmann JK Cheng Z, Davis C, et al. Targeted microbubbles for imaging tumor angiogenesis: assessment of whole-body biodistribution with dynamic MicroPET imaging in mice. Radiology (in press).
21. Weller GE, Villanueva FS, Tom EM, Wagner WR. Targeted ultrasound contrast agents: in vitro assessment of endothelial dysfunction and multi-targeting to ICAM-1 and sialyl Lewisx. Biotechnol Bioeng 2005;92:780–788.
22. Bhatia SK, King MR, Hammer DA. The state diagram for cell adhesion mediated by two receptors. Biophys J 2003;84:2671–2690.
23. Eniola AO, Willcox PJ, Hammer DA. Interplay between rolling and firm adhesion elucidated with a cell-free system engineered with two distinct receptor-ligand pairs. Biophys J 2003;85:2720–2731.

Radiology 2008

This is your reprint order form or pro forma invoice

(Please keep a copy of this document for your records.)

Reprint order forms and purchase orders or prepayments must be received 72 hours after receipt of form either by mail or by fax at 410-820-9765. It is the policy of Cadmus Reprints to issue one invoice per order. **Please print clearly**.

Author Name _____
Title of Article _____
Issue of Journal_____ Reprint # _____ Publication Date _____
Number of Pages_____ KB # _____ Symbol Radiology
Color in Article? Yes / No (Please Circle)

Please include the journal name and reprint number or manuscript number on your purchase order or other correspondence.

Order and Shipping Information

Reprint Costs (Please see page 2 of 2 for reprint costs/fees.)

_____ Number of reprints ordered $_____
_____ Number of color reprints ordered $_____
_____ Number of covers ordered $_____
Subtotal $_____
Taxes $_____

(*Add appropriate sales tax for Virginia, Maryland, Pennsylvania, and the District of Columbia or Canadian GST to the reprints if your order is to be shipped to these locations*.)

First address included, add $32 for each additional shipping address $_____

TOTAL $_____

Shipping Address (cannot ship to a P.O. Box) Please Print Clearly

Name _____
Institution _____
Street _____
City _____ State _____ Zip _____
Country _____
Quantity_____ Fax _____
Phone: Day _____ Evening _____
E-mail Address _____

Additional Shipping Address* (cannot ship to a P.O. Box)

Name _____
Institution _____
Street _____
City _____ State _____ Zip _____
Country _____
Quantity _____ Fax _____
Phone: Day _____ Evening _____
E-mail Address _____
** Add $32 for each additional shipping address*

Payment and Credit Card Details

Enclosed: Personal Check _____
Credit Card Payment Details _____
Checks must be paid in U.S. dollars and drawn on a U.S. Bank.

Credit Card: __ VISA __ Am. Exp. __ MasterCard
Card Number _____
Expiration Date_____
Signature: _____

Please send your order form and prepayment made payable to:

Cadmus Reprints
P.O. Box 751903
Charlotte, NC 28275-1903

Note: Do not send express packages to this location, PO Box.
FEIN #:541274108

Invoice or Credit Card Information

Invoice Address Please Print Clearly
Please complete Invoice address as it appears on credit card statement

Name _____
Institution _____
Department _____
Street _____
City _____ State _____ Zip _____
Country _____
Phone _____ Fax _____
E-mail Address _____

Cadmus will process credit cards and *Cadmus Journal Services* will appear on the credit card statement.

If you don't mail your order form, you may fax it to 410-820-9765 with your credit card information.

Signature _____ Date _____

Signature is required. By signing this form, the author agrees to accept the responsibility for the payment of reprints and/or all charges described in this document.

RB-9/26/07

Radiology 2008

Black and White Reprint Prices

Domestic (USA only)						
# of Pages	50	100	200	300	400	500
1-4	$221	$233	$268	$285	$303	$323
5-8	$355	$382	$432	$466	$510	$544
9-12	$466	$513	$595	$652	$714	$775
13-16	$576	$640	$749	$830	$912	$995
17-20	$694	$775	$906	$1,017	$1,117	$1,220
21-24	$809	$906	$1,071	$1,200	$1,321	$1,471
25-28	$928	$1,041	$1,242	$1,390	$1,544	$1,688
29-32	$1,042	$1,178	$1,403	$1,568	$1,751	$1,924
Covers	$97	$118	$215	$323	$442	$555

International (includes Canada and Mexico)						
# of Pages	50	100	200	300	400	500
1-4	$272	$283	$340	$397	$446	$506
5-8	$428	$455	$576	$675	$784	$884
9-12	$580	$626	$805	$964	$1,115	$1,278
13-16	$724	$786	$1,023	$1,232	$1,445	$1,652
17-20	$878	$958	$1,246	$1,520	$1,774	$2,030
21-24	$1,022	$1,119	$1,474	$1,795	$2,108	$2,426
25-28	$1,176	$1,291	$1,700	$2,070	$2,450	$2,813
29-32	$1,316	$1,452	$1,936	$2,355	$2,784	$3,209
Covers	$156	$176	$335	$525	$716	$905

Minimum order is 50 copies. For orders larger than 500 copies, please consult Cadmus Reprints at 800-407-9190.

Reprint Cover

Cover prices are listed above. The cover will include the publication title, article title, and author name in black.

Shipping

Shipping costs are included in the reprint prices. Domestic orders are shipped via UPS Ground service. Foreign orders are shipped via a proof of delivery air service.

Multiple Shipments

Orders can be shipped to more than one location. Please be aware that it will cost $32 for each additional location.

Delivery

Your order will be shipped within 2 weeks of the journal print date. Allow extra time for delivery.

Color Reprint Prices

Domestic (USA only)						
# of Pages	50	100	200	300	400	500
1-4	$223	$239	$352	$473	$597	$719
5-8	$349	$401	$601	$849	$1,099	$1,349
9-12	$486	$517	$852	$1,232	$1,609	$1,992
13-16	$615	$651	$1,105	$1,609	$2,117	$2,624
17-20	$759	$787	$1,357	$1,997	$2,626	$3,260
21-24	$897	$924	$1,611	$2,376	$3,135	$3,905
25-28	$1,033	$1,071	$1,873	$2,757	$3,650	$4,536
29-32	$1,175	$1,208	$2,122	$3,138	$4,162	$5,180
Covers	$97	$118	$215	$323	$442	$555

International (includes Canada and Mexico))						
# of Pages	50	100	200	300	400	500
1-4	$278	$290	$424	$586	$741	$904
5-8	$429	$472	$746	$1,058	$1,374	$1,690
9-12	$604	$629	$1,061	$1,545	$2,011	$2,494
13-16	$766	$797	$1,378	$2,013	$2,647	$3,280
17-20	$945	$972	$1,698	$2,499	$3,282	$4,069
21-24	$1,110	$1,139	$2,015	$2,970	$3,921	$4,873
25-28	$1,290	$1,321	$2,333	$3,437	$4,556	$5,661
29-32	$1,455	$1,482	$2,652	$3,924	$5,193	$6,462
Covers	$156	$176	$335	$525	$716	$905

Tax Due

Residents of Virginia, Maryland, Pennsylvania, and the District of Columbia are required to add the appropriate sales tax to each reprint order. For orders shipped to Canada, please add 7% Canadian GST unless exemption is claimed.

Ordering

Reprint order forms and purchase order or prepayment is required to process your order. Please reference journal name and reprint number or manuscript number on any correspondence. You may use the reverse side of this form as a proforma invoice. Please return your order form and prepayment to:

Cadmus Reprints
P.O. Box 751903
Charlotte, NC 28275-1903

Note: Do not send express packages to this location, PO Box.
FEIN #:541274108

Please direct all inquiries to:

Rose A. Baynard
800-407-9190 (toll free number)
410-819-3966 (direct number)
410-820-9765 (FAX number)
baynardr@cadmus.com (e-mail)

Reprint Order Forms and purchase order or prepayments must be received 72 hours after receipt of form.